Conformational free energy of melts of ring-linear polymer blends

Gopinath Subramanian[1,*] and Sachin Shanbhag[2,†]
[1]*Scientific Computation Research Center, Rensselaer Polytechnic Institute, Troy, New York 12180-3590, USA*
[2]*Department of Scientific Computing, Florida State University, Tallahassee, Florida 32306-4120, USA*
(Received 23 July 2009; published 21 October 2009)

The conformational free energy of ring polymers in a blend of ring and linear polymers is investigated using the bond-fluctuation model. Previously established scaling relationships for the free energy of a ring polymer are shown to be valid only in the mean-field sense, and alternative functional forms are investigated. It is shown that it may be difficult to accurately express the total free energy of a ring polymer by a simple scaling argument, or in closed form.

DOI: 10.1103/PhysRevE.80.041806 PACS number(s): 83.80.Tc, 02.70.Uu

I. INTRODUCTION

From a topological standpoint, ring polymers (RPs, or rings) are linear polymers (LPs, or linears) with one additional constraint—the ends of an RP are constrained to overlap with each other. This single extra constraint decreases the conformational degrees of freedom and introduces significant qualitative changes in the static properties of an LP that is cyclized [1]. The reduction in the number of conformational degrees of freedom translates directly to a change in the entropy, and by extension, the free energy. There is renewed interest in engineering circular proteins by cyclizing the peptide backbone, motivated by the possibility of manipulating the folding stability [2]. By aiming to reduce the entropy of the unfolded state by connecting the N and C termini of a linear protein, the process of unfolding is rendered less favorable. Unlike LPs, RPs can also undergo catenation (formation of "Olympic rings"), which has also been shown to have applications in stabilizing folded protein structures [3].

While the properties of RPs in dilute solution have been studied before [4,5], it is not surprising that the static properties of RPs *in a melt* are also qualitatively different from those of LPs. Uncatenated RPs tend to adopt more compact conformations than their linear counterparts, and exhibit a relationship between molecular weight and size that is different from LPs [6–9]. Besides catenation, RPs exhibit another conformational feature that is not displayed by LPs—the ability to form knots. An analysis of knots and geometry in double stranded cyclic DNA, which is also an RP is a very active area of research with potential applications in enzymology [10–12].

Unknotted and uncatenated RPs are therefore the simplest ring structures. Although they are devoid of geometrical complexities that arise from catenation and knotting, their properties—both static and dynamic—are still not well established. A significant experimental challenge in preparing a melt of RPs is controlling the level of contamination by LPs [13]. Trace quantities of LPs are left over even after herculean purification steps, and they thread through the RPs causing them to swell, thereby affecting the static properties [14], and constrain their motion resulting in lower diffusivity [15–17], and dramatically longer characteristic relaxation times [13,18]. Thus, ring-linear blends (RLBs) are of practical interest as most experimental data on pure RPs are in fact data on RLBs, and an exploration of these systems provides the closest computational analog of real RP melts [9,14,19].

To explain the non-Gaussian dependence of the radius of gyration R on the number of monomers N in an uncatenated RP melt, Cates and Deutsch invoked a "Flory-like" self-consistent argument and represented the free energy of noncatenated RPs as [7]

$$F(R) = \frac{R^3}{N} + \frac{N}{R^2}, \tag{1}$$

where the first term is proportional to the number of RPs that pervade a sphere of R^3, and is proposed in order to capture the increase in free energy arising from the noncatenation constraint. The second term denotes the Gaussian free-energy increase that favors the expansion of the coil. Minimizing the free energy leads to a mean size $\bar{R} \sim N^{2/5}$. Subsequent simulations using the bond-fluctuation model [20,21] and neutron scattering experiments [22] seem to support this exponent, while other simulations [23–26] and experimental studies [27] seem to support values of the exponent closer to $\nu = 1/3$. The difference in exponents from different studies might be in part due to the very slow approach to asymptotic behavior, as observed by Obukhov *et al.* [26]. For RLBs, in the regime where the concentration of the RPs is considered "semidilute," and an RP is able to perceive the presence of other RPs, this argument can be expanded as [14]

$$F(R) = F_c(R) + F_g(R), \tag{2}$$

$$F_c(R) = \phi_R \frac{R^3}{N}, \tag{3}$$

$$F_g(R) = \frac{N}{R^2}, \tag{4}$$

where ϕ_R/ϕ and ϕ_L/ϕ are the relative compositions of the RP and LPs, respectively, with $\phi = \phi_R + \phi_L$. F_c and F_g are the contributions to the free energy from the noncatentation con-

*gsub@scorec.rpi.edu
†sshanbhag@fsu.edu

straint and the Gaussian nature of the RPs, respectively. Minimizing the free energy by setting $dF/dR=0$ leads to

$$\bar{R} \sim \phi_R^{-1/5} N^{2/5}. \tag{5}$$

The exponents obtained in Eq. (5) are a direct result of the form of Eqs. (2)–(4), which are modified forms of Eq. (1). The scaling model of Iyer *et al.* [14] is more general than Eq. (5): it predicts that $\bar{R} \sim \phi_R^{2\nu-1} N^{\nu}$, even when ν is different from 2/5.

In an attempt to computationally ascertain the applicability of Eqs. (2)–(4), conformations of individual RPs in an RLB melt are examined in this paper. In particular, this work shows that the expression used in Eq. (3) is valid only in the mean sense, as evidenced by the validity of Eq. (5), and seeks to examine an alternate expression for F_c. While the molecular weights of the polymers considered in the present work might not be large enough to accurately predict asymptotic behavior, this study is intended to establish the computational framework for analyzing the statistics of asymptotically large polymers.

II. MODEL AND METHODS

A. Theoretical framework

The free energy F of an athermal RP in a melt is purely entropic, and may be expressed as

$$\frac{F(R)}{k_B T} = -\ln \Omega(R), \tag{6}$$

where $\Omega(R)dR$ is the number of conformations with radius of gyration between R and $R+dR$. Given the molecular weight and the composition of an RLB, the value of $\Omega(R|N;\phi_R)$ is related to the probability density function of R as

$$P(R|N;\phi_R) = \frac{\Omega(R|N;\phi_R)}{\int \Omega(R|N;\phi_R)dR} = \frac{\Omega(R|N;\phi_R)}{\lambda(N,\phi_R)Z_L(N)}, \tag{7}$$

where $P(R|N;\phi_R)dR$ represents the fraction of RPs with a radius of gyration between R and $R+dR$.

Dropping the denominator $k_B T$, the free energy of an RP may thus be obtained as

$$F(R|N;\phi_R) = -\ln[\lambda(N,\phi_R)P(R|N;\phi_R)] - \ln Z_L(N), \tag{8}$$

where $Z_L(N)$ is the partition function of an LP with N beads, and is indicative of the total number of conformations that it may adopt. Previous simulations [9] indicate that the static properties of LPs are unaffected by the composition of the RPs in the blend, and hence Z_L is assumed to be independent of ϕ_R. The partition function $Z_L(N)$ does not enter into calculations presented in this paper explicitly, beyond an additive constant, which cancels out when we calculate F_c. (However, knowledge of Z_L is required to directly compare the free energies of two different molecular weights.)

$\lambda(N,\phi_R)$ is the probability with which an LP adopts a conformation in which its ends overlap. The second equality in Eq. (7) offers a more tractable computational route to calculate $P(R)$, and will be employed in this paper. Computation of $F(R)$ thus requires knowledge of (a) $\lambda(N,\phi_R)$—the probability with which an LP adopts a conformation indistinguishable from that of an RP, which occurs when its ends essentially overlap, and (b) $P(R)$—the probability density function of RPs characterized using the radius of gyration R as the macrostate variable. These quantities are expected to change with the relative fraction of RPs in the polymer melt, as indicated by Eq. (3).

The free-energy contribution of the catenation constraint F_c may be computed as

$$F_c(R|N;\phi_R) = F(R|N;\phi_R) - F_g(R|N), \tag{9}$$

where the expression for $F_g(R)$ is the free energy of Gaussian RPs, which as shown later may be computed either analytically or via simulation, and is independent of ϕ_R.

To obtain the quantities $\lambda(N,\phi_R)$, $P(R)$, and $F_g(R)$, simulations were executed using a lattice model with varying N and RP concentrations. The model used for these studies is described in some detail in the following sections.

B. Bond fluctuation model

The bond-fluctuation model (BFM) proposed by Shaffer [28] was used to simulate the RLB systems considered in this study. To distinguish it from the original bond-fluctuation model [29,30], it is referred to as S-BFM. In the S-BFM, polymers are grown on a simple cubic lattice, where lattice points represent beads. The system is subject to the following three constraints: (1) excluded volume constraint: enforced by forbidding multiple occupancy of lattice sites; (2) chain connectivity constraint: enforced by restricting the length of the bond connecting two consecutive beads to the set of values $\{1,\sqrt{2},\sqrt{3}\}$; (3) chain uncrossability constraint: enforced by forbidding bond midpoints from intersecting.

The polymers are then moved by choosing a bead at random and attempting to move it to one of its six nearest neighbors. A trial move is accepted if it does not violate the constraints described above. n_R noncatenated RPs, each having N monomers were grown on a cubic lattice in a cubic simulation box of side L_{box} lattice units with periodic boundary conditions. These RPs were then shuffled for approximately $25\,000Nn_R$ trial moves to ensure that they were distributed evenly in space. Following this, n_L LPs with the same number of beads per molecule N were then grown as random walks that avoided all occupied lattice sites and did not violate any of the three constraints. In order to simulate meltlike behavior, the total fractional occupancy of the simulation box was maintained at $\phi=\phi_R+\phi_L=0.5$. Here, $\phi_R=n_R N/L^3$ and $\phi_L=n_L N/L^3$ represent the fractional occupancy of RPs and LPs, respectively.

The LPs thus grown were then shuffled for approximately $t=25\,000Nn_L$ trial moves while the RPs were held frozen, with the three constraints enforced. The initial configuration thus obtained was equilibrated by attempting to move a randomly selecting a bead (regardless of whether it belonged to an RP or an LP) subject to the three constraints. $(n_L+n_R)N$ trial moves were taken to constitute 1 MC time step. To determine if the system was equilibrated, the autocorrelation

function of the end-to-end vector (for LPs) and the diametrical vector (for RPs) were monitored. These autocorrelation functions are defined by

$$p_i(t) = \frac{\langle \mathbf{r}_{ee}(t) \cdot \mathbf{r}_{ee}(0) \rangle}{\langle r_{ee}^2(0) \rangle}, \tag{10}$$

where for LPs ($i=L$), p_L is obtained by setting $\mathbf{r}_{ee}(t)=\mathbf{r}_N(t)-\mathbf{r}_1(t)$, the vector connecting bead 1 to bead N of a polymer chain. For RPs ($i=R$), p_R is obtained by setting $\mathbf{r}_{ee}(t)=\mathbf{r}_{N/2}(t)-\mathbf{r}_1(t)$, the "diametrical" vector connecting bead 1 to bead $N/2$ of an RP. The system was taken to be equilibrated when both p_L and p_R had dropped below 0.1. The time taken for a simulation box to fully equilibrate was assumed to be approximately equal to the relaxation time τ_b. Polymer conformational data from a simulation box was considered to be statistically independent only if the time between sampling was at least τ_b.

C. Classifying RPs and estimating probabilities

A fully equilibrated simulation box containing both RPs and LPs was taken to be the starting point for estimating the probability density function $P(R)$. The RPs present in this simulation box are referred to as the "true rings," for clarity. The polymer beads in the simulation box were then moved around in the manner described above, subject to the three constraints.

At the end of *each time step*, the LPs in the simulation box were examined one by one. If it were possible to connect the end beads of an LP by a valid lattice bond vector (cube edge, face diagonal, or solid diagonal) that did not lead to crossing of pre-existing bonds (to preserve the enforcement of the uncrossability constraint), the LP was considered to be indistinguishable from an RP. The closing bond was added to convert the LP into an RP, and such an RP is referred to as a "false ring." The conformational information of this false ring was recorded. It was then examined for self-knotting using the annealing algorithm, and for catenation with the true rings using the linking number algorithm (see Sec. II D for details). This implementation of the catenation constraint does not inspect catenation between two false rings. Based on the state of knotting and catenation, the false rings thus obtained were classified as either of (a) valid—V, (b) only self-knotted—S, (c) only catenated—C, or (d) both self-knotted and catenated—SC. These categories correspond to the regions shown schematically in Fig. 1. The superscripts V, S, C, and SC are used to distinguish each class of false rings, and the superscript A is used to designate the superset of all the false rings, i.e., $A=\mathrm{V}\cup\mathrm{S}\cup\mathrm{C}\cup\mathrm{SC}$, where V, S, C, and SC are disjoint sets.

The closing bond of the false ring was then removed, converting it back into an LP, and the simulation was allowed to proceed. For each class, the frequency with which LPs form false rings leads to an estimate of $\lambda(N,\phi_R)$, and the conformational information of the false rings collected over the course of the simulation provides an estimate of the probability density function $P(R)$.

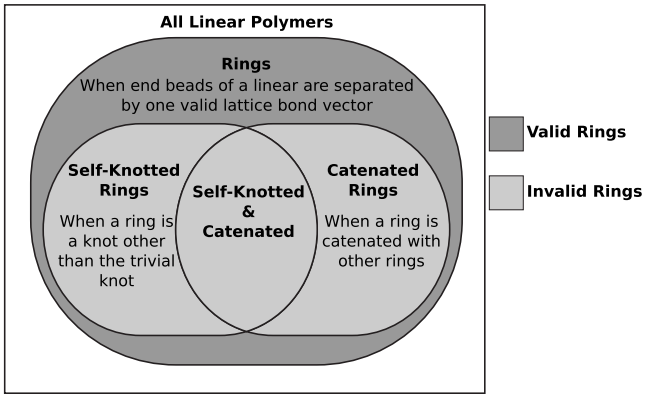

FIG. 1. Venn diagram indicating the four categories of ring polymers (RPs)—(a) valid, (b) self-knotted, (c) catenated, and (d) self-knotted and catenated. The superscripts V, S, C, and SC are, respectively, used for each of these four categories. The superscript A is used to denote the superset of all false RPs. In other words, $\mathrm{A}=\mathrm{V}\cup\mathrm{S}\cup\mathrm{C}\cup\mathrm{SC}$, where V, S, C, and SC are disjoint sets.

D. Identifying knotting and catenation

In this study, the annealing and linking number algorithms are used to identify configurations of false rings which are knotted and catenated, respectively.

1. Annealing algorithm

Given a simulation snapshot, the annealing algorithm [31,32] prescribes a method to identify the primitive paths—the shortest contour that does not violate topological constraints—of all the polymers in the system. This information may be used to probe whether an RP is knotted or not. Alternatively, it is possible to use knot polynomials such as the Jones polynomial [33] to study the existence and complexity of knots in RPs. However, an analysis of the primitive path network which the annealing algorithm generates can diagnose some pathological knots that knot polynomials could in principle miss, because at time of writing, the question of whether there exists a nontrivial knot having the same Jones polynomial of an unknot is an open one [34].

The annealing algorithm, along with an examination of the parameters used is described in detail elsewhere [9], but is summarized in this section. The ends of LPs and a pair of consecutive beads belonging to an RP in the simulation box are held fixed while the other beads are free to move. The intramolecular excluded volume constraint *between consecutive beads* is turned off while the intermolecular excluded volume constraint is maintained. This is done to facilitate the shrinkage of the chain contours while maintaining their noncrossability with other chains. The probability with which moves that increase the primitive path length are accepted is decreased according to the expression

$$p_{acc}(t) = \min\left\{1, \exp\left[-A\Delta L\left(\frac{t}{\tau_{\text{anneal}}}\right)^2\right]\right\}, \tag{11}$$

where ΔL is the change in contour length (positive or negative) due to a trial move and τ_{anneal} is the duration of the annealing process. In the present study, the parameters were

set as $A=16$ and $\tau_{\text{anneal}}=10\tau_e$, where $\tau_e \approx 5000$ MCS is the Rouse time corresponding to an entanglement segment [35,36].

Upon completion of annealing, an RP that is not knotted with itself or catenated with other RPs should collapse into a single point. However, the lattice structure adopted for these simulations allows such an RP to collapse into a triangle, and no further. This is because of the bond uncrossability constraint that is enforced. Thus, unknotted and noncatenated RPs would collapse into a triangle with a maximum contour length of $3\sqrt{2}$ (three bonds along the face diagonals of the lattice). These cases are illustrated in Fig. 2(a). If, on the other hand an RP were "self-knotted," the annealing algorithm would be incapable of shrinking its contour length beyond a certain point without violating the three constraints, and would yield conformations like the one shown in Fig. 2(b). This conformation is the so-called trefoil knot. Such knotted conformations have contour lengths greater than $3\sqrt{2}$. Third, if two RPs were catenated, the annealing algorithm would at best reduce the contour length of one of the two RPs to $3\sqrt{2}$ [Fig. 2(c)].

This property may be exploited to determine whether a false ring is knotted with itself or catenated. To test for catenation [Fig. 2(c)] all the RPs in the system have to be included in the annealing operation, which takes on the order of a few hours of CPU time on a single 3 GHz CPU. However, an examination of the primitive path of false rings, *inspected one at a time* is sufficient to reveal self-knotting. Computationally, the operation is very inexpensive, and requires a few seconds of CPU time. Besides, there exist more efficient methods to check whether two RPs are linked. Thus, in this study, annealing is only used to identify self-knotting.

2. Linking number algorithm

The Gauss linking number of two RPs is an invariant [37]. Linking numbers of any two RPs are computed by counting the number of intersections in a two-dimensional projection of the two links. Two RPs (nearest periodic images [38]) isolated from the rest of the system are taken as inputs to the linking number algorithm. The RPs are then translated by equal amounts to the new coordinates $\mathbf{r}_j^i = (x_{i,j}, y_{i,j}, z_{i,j})$, (where the index i is either 1 or 2, and the index j denotes the bead number), satisfying the condition

$$\min\{x_{i,j}, y_{i,j}, z_{i,j}\} = 1, \quad \forall\, i \in [1,2], \;\; j \in [1,N]. \tag{12}$$

This is equivalent to translating (without rotating) the original coordinate system in such a way that for the two polymers under consideration, the smallest coordinate of any of their beads is unity (in lattice units). While the choice of unity is somewhat arbitrary, the translation of the coordinate system is done to avoid large numbers when computing the linking number.

The positive nonzero coordinates of bead j from polymer i are then projected onto a plane according to

$$X_{i,j} = x_{i,j} + \frac{z_{i,j}}{L'+1},$$

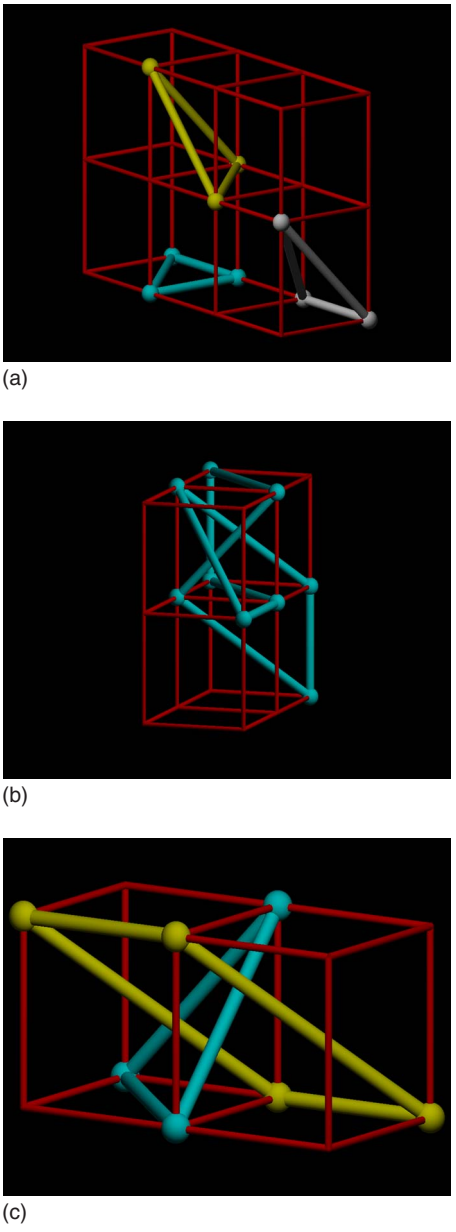

FIG. 2. (Color online) The result of annealing on different kinds of ring polymers (RPs): (a) valid RPs, (b) a self-knotted RP (Trefoil knot), (c) two catenated RPs. After annealing, valid, noncatenated RPs attain a contour length of at most $3\sqrt{2}$. If two RPs are catenated, at least one of them attains a contour length greater than $3\sqrt{2}$.

$$Y_{i,j} = y_{i,j} + \frac{z_{i,j}}{2(L'+1)}, \tag{13}$$

where L' is the side of the cubic box drawn to contain both RPs, and is defined as

$$L' = \max\{x_{i,j}, y_{i,j}, z_{i,j}\} + 1, \quad \forall\, i \in [1,2], \;\; j \in [1,N]. \tag{14}$$

This transformation is a variant of the transformation used by Lua *et al.* [39,40], and guarantees that (a) no two polymer beads are projected onto the same point and (b) no two pro-

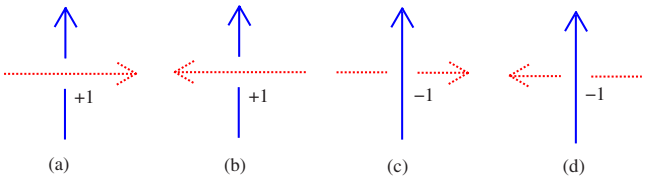

FIG. 3. (Color online) Procedure for calculating linking number.

jected bonds are collinear. Each projected chain is then assigned a direction. The direction of the projection was arbitrarily chosen to be in the direction of increasing bead numbers. The intersection points on the projection were identified and assigned either +1 or −1 according to the schematic shown in Fig. 3. The number of intersections of each type was also counted, and the linking number was computed as $(n_a+n_b-n_c-n_d)/2$, where n_x is the number of crossings of type x.

In general, a linking number of zero implies that the two RPs in question are not catenated, although notable exceptions such as the Whitehead link [41] exist. For purposes of this study, the fraction of catenated RPs declared as uncatenated by the liking number algorithm was found to be negligible (see appendix) and thus, any two RPs with a linking number of zero were taken to be noncatenated.

III. RESULTS

A. Preliminaries

In this study, systems with $N \in \{10,30,80,150,200\}$ were considered. For each value of N, the fraction of RPs considered were $\phi_R \in \{0.025,0.250,0.475\}$. The values of ϕ_R were chosen to mimic different environments, ranging from mostly LPs to mostly RPs. For reference, for the S-BFM, the number of beads corresponding to an entanglement strand in LPs is $N_e \approx 30$ [30,32]. Thus, even the longest polymers simulated here are smaller than seven entanglements long. While longer polymers with approximately 20 entanglements and larger have been simulated with this model in earlier work [23,28,32], simulations larger than the ones considered in this study become prohibitively expensive, because the probability with which an LP forms a false ring, valid or otherwise, λ^A decreases rapidly with increasing molecular weight N. This is not surprising because as N increases, the probability with which the ends of an LP come within one lattice spacing of each other decreases, as the LP has a far greater number of conformational degrees of freedom to explore. When the normal distribution is used to determine the probability that a Gaussian LP has a vanishing end-to-end vector and forms a Gaussian RP, it is expected that $\lambda^A \sim N^{-3/2}$, which is observed in Fig. 4. The actual fit obtained is $\lambda^A \approx 2.06N^{-1.56}$. The probability of forming a valid ring $\lambda^V < \lambda^A$, and unlike λ^A it decreases with increasing ϕ_R.

As the fraction of true rings in the melt ϕ_R increases, an LP has a greater likelihood of threading through a true ring before its ends are within one lattice spacing of each other, thereby increasing the probability of catenation, and decreasing the probability of forming a valid ring. It may be observed that at the lowest value of ϕ_R, where an LP is surrounded largely by other LPs, the behavior of $\lambda^V(N,\phi_R=0.025)$ is similar to Gaussian RPs or λ^A. This is because the strength of the catenation constraint which increases with ϕ_R is weakest in this case.

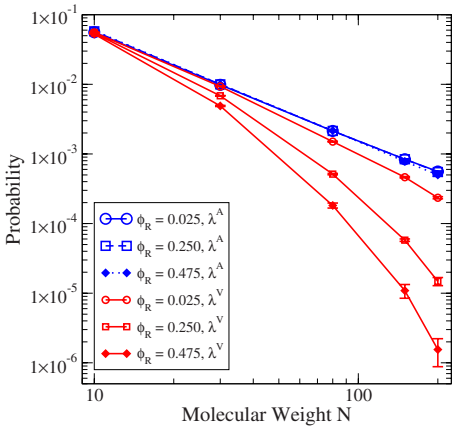

FIG. 4. (Color online) The probability of a linear forming a ring λ^A decreases with increasing molecular weight N, and is independent of ϕ_R, the fraction of RPs in the melt. On the other hand, the probability of a linear forming a *valid* ring, λ^V, decreases as either of N or ϕ_R increase. The fit obtained is $\lambda^A \approx 2.06N^{-1.56}$

If $\mathbf{r}_i$ denotes the coordinates of the ith bead, then the internal distribution of distances between beads may be obtained by examining

$$r^2(n|N;\phi_R) = \langle(\mathbf{r}_i - \mathbf{r}_{i+n}) \cdot (\mathbf{r}_i - \mathbf{r}_{i+n})\rangle, \tag{15}$$

where the average is computed over false rings of a particular type formed during the course of the simulation. Figure 5 shows a representative plot of $r^2(n|N;\phi_R)$ for $N=150$ and $\phi_R=0.250$. It is seen that on average, the false rings that are only self-knotted are the smallest. On the other hand, the false rings that are only catenated with true rings are the largest. The self-knotted and catenated false rings are smaller

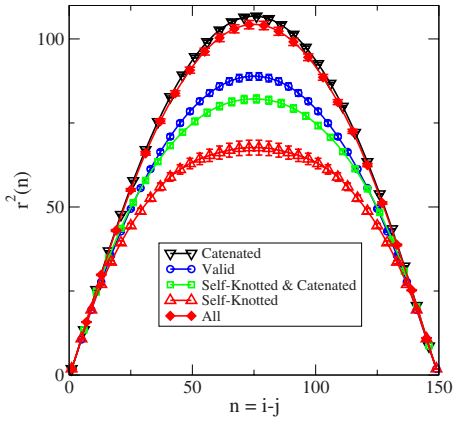

FIG. 5. (Color online) The average distance between beads of the 4 different classes of polymers for $N=150$. As expected, the catenated polymers are the largest, and the self-knotted polymers are the smallest. This plot is representative of the trend observed over all values of N and ϕ_R.

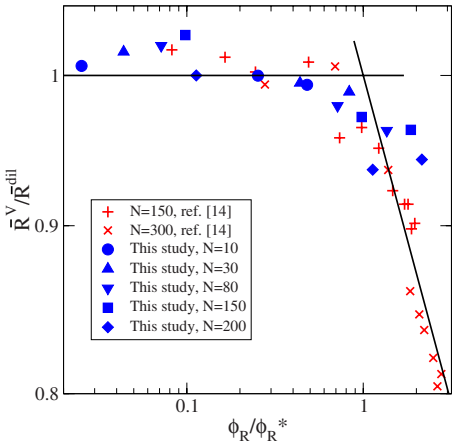

FIG. 6. (Color online) The average radius of gyration of valid rings, $\bar{R}^V$ measured in this study, along with previously published data on ring-linear blends, according to the scaling established in [14].

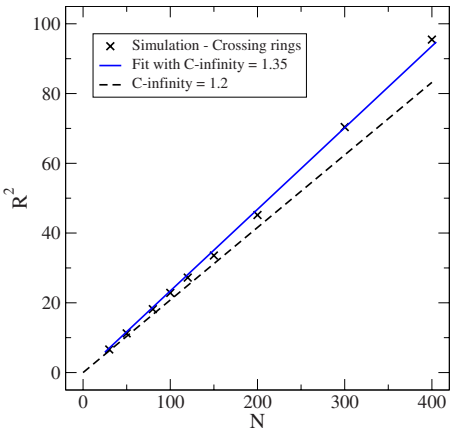

FIG. 7. (Color online) Simulation data on rings that are allowed to cross each other. The solid line fitted is $R^2=C_\infty(N-1)b^2/12$ with $C_\infty=1.35$, and $b^2=2.08$. The broken line uses $C_\infty=1.2$.

than the purely catenated variety, and larger than the purely self-knotted variety.

Figure 6 shows the average radius of gyration of valid rings measured in these simulations, along with the data obtained previously [14]. It is seen that $\bar{R}^V$ decreases with increasing ϕ_R, which results from the noncatenation constraint that causes RPs to shrink in the presence of other RPs.

B. Free-energy contribution of Gaussian rings

Computing the quantity $F_g(R)$ requires knowledge of the probability density function of R (or equivalently, the probability density function of R^2) of Gaussian rings, denoted here as $P_g(R)$. It may be computed in either of two ways.

(1) Analytically, an expression for $P_g(R^2)$ in three dimensions has been derived as [42]

$$P_g(R^2) = \frac{1}{2\pi}\int_{-\infty}^{\infty} K(s)\exp[-isR^2]ds,$$

$$K(s) = \left[\frac{Y/2}{\sin(Y/2)}\right]^3,$$

$$Y = \sqrt{\frac{2isN_K}{3}}, \tag{16}$$

where the number of Kuhn steps is N_K, and the Kuhn step length is assumed to be unity. It should be pointed out that this relationship does not require $N_K \gg 1$.

(2) Alternatively, the RPs in the BFM are known to display Gaussian statistics, if bond uncrossability (constraint 3 in Sec. II B) is switched off [43]. By running a simulation consisting of pure rings which are allowed to cross each other, $P_g(R^2)$ may be obtained.

In this study we used both these methods. To obtain the relationship between the number of beads N and the number of Kuhn steps N_K, we used $(N_K-1)=(N-1)/C_\infty$, where C_∞ is the characteristic ratio defined as $R^2=C_\infty(N-1)b^2/12$, with b^2 denoting the average bond length. By fitting simulation data on crossing RPs (which obey Gaussian statistics), we obtain $C_\infty=1.35$ with $b^2=2.08$, as shown in Fig. 7. This value of C_∞ is slightly larger than the corresponding value for crossing LPs for which it is approximately equal to 1.2. Using the value of $C_\infty=1.35$, in Eq. (16) we obtain the probability distribution function of R^2 analytically, for the molecular weights considered in this study. These analytical results (method 1) are overlaid with histograms of the probability distribution function obtained from a direct simulation of crossing RPs (method 2) in Fig. 8. While the agreement between the two methods is largely reasonable, it may be seen that regions far away from the maxima on either side are not sampled perfectly by method 2. This underestimation at small and large values of R relative to $\bar{R}$ is responsible for the overestimation of the probability near $R \approx \bar{R}$. It may also be seen that the most probable R obtained from both methods are slightly different. This may be due to small errors in fitting present when obtaining C_∞.

If the catenation constraint is absent or suppressed, the Cates-Deutsch argument given by Eq. (1) implies that the free energy of the RPs is given by the free energy of Gaussian rings. To test this implication, we calculated the free energy of *all the false rings* formed during the course of the simulation via Eq. (8), which includes contributions from self-knotted and catenated conformations. When plotted with the free energy of Gaussian rings obtained from the analytical expression for $P(R)$ (as shown by solid lines in Fig. 8), we obtain Fig. 9. Note that the curves, unlike the distribution of the end-to-end vectors, are not symmetric about the minima, both in the simulations and analytical expression. Further, the simulation curves are independent of ϕ_R, as expected since contributions from catenated conformations, which increase with ϕ_R, are included in this figure. The overall agreement validates the first part of the Cates-Deutsch conjecture, and indicates that if the catenation constraint is removed, the rings formed display characteristics of Gaussian rings. The small discrepancy at values of R that are far removed from the minimum are associated with sampling errors, which also manifest in Fig. 8.

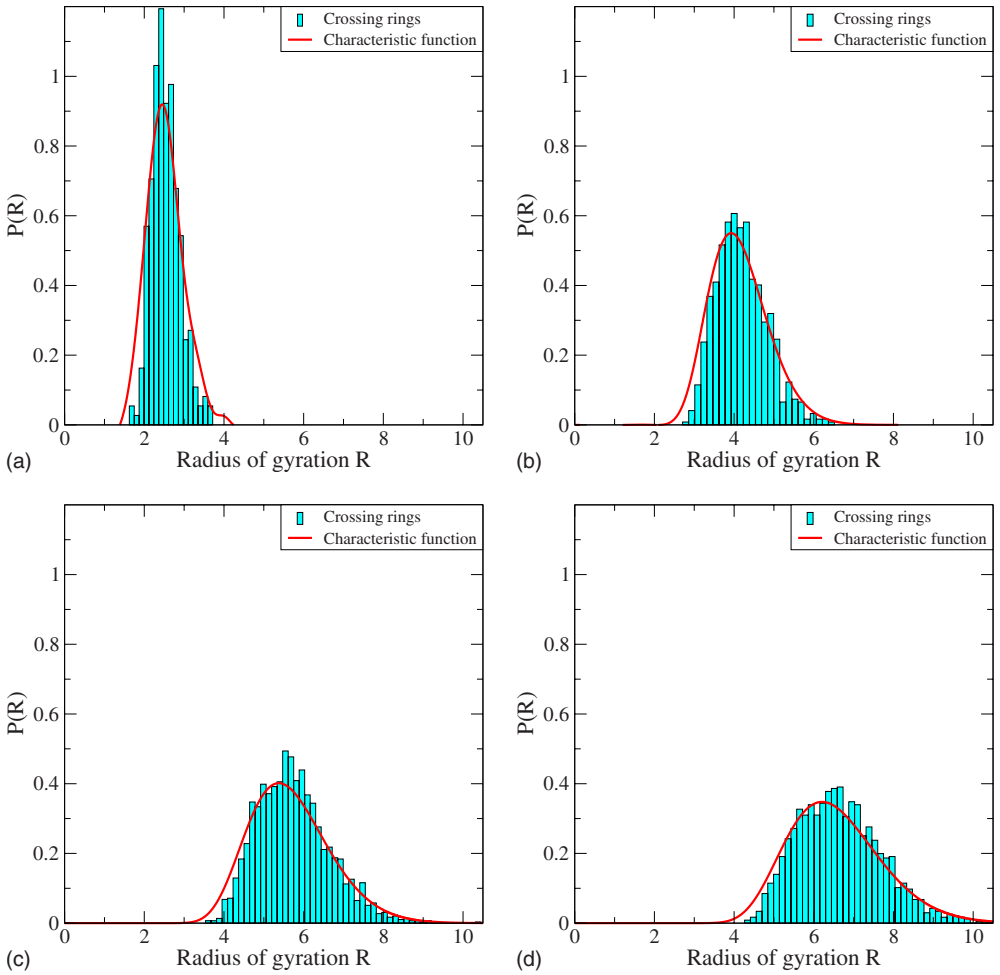

FIG. 8. (Color online) The PDF of R^2 obtained by numerically integrating the characteristic function, and from crossing S-BFM simulations for (a) $N=30$, (b) 80, (c) 150, and (d) 200. The results of integrating Eq. (16) have been rescaled to S-BFM lattice units. Also shown is the PDF of R of all false rings.

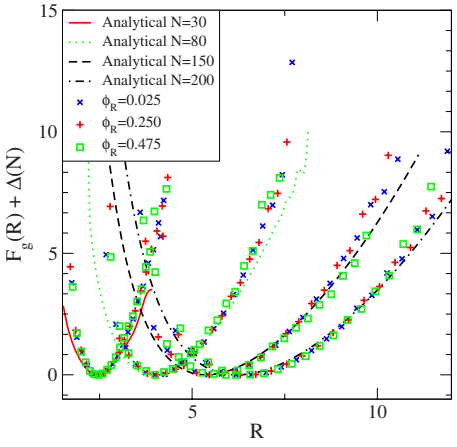

FIG. 9. (Color online) The Gaussian free energy as a function of radius of gyration $F_g(R)$ plotted for different molecular weights. The Gaussian free energy with the analytical and simulation curves were shifted by an amount $\Delta(N)$ along the Y axis, and $N=10$ omitted.

IV. DISCUSSION

Having obtained the free energy of Gaussian rings, and the free energy of valid rings, the free energy of catenation was computed as $F_c(R)=F(R)-F_g(R)$. In the expressions for $F(R)$ and $F_g(R)$, the natural logarithm of the partition function, $\log Z_L$, appears as an additive constant, which cancels out when we take the difference, and thus, does not play a role in determining $F_c(R)$. Thus, we choose $Z_L=1$ in this study. However, if we were to directly compare the free energies of two different molecular weights, it would be necessary to know the actual value of Z_L.

The values of $F_g(R)$ computed from (a) The characteristic function in Eqs. (16), (b) simulations of crossing rings and (c) all false rings formed during the course of this study agree reasonably well with each other. To eliminate the effect of inadequate sampling, and the fitting errors present in obtaining C_∞, we chose to use the PDF of all false rings to obtain $F_g(R)$, as we had the best statistics for this case.

The catenation constraint is operative only in the "semidilute" regime, where conformations of RPs overlap. The overlap concentration of RPs in ring-linear blends ϕ_R^* that determines the boundary between the dilute and semidilute

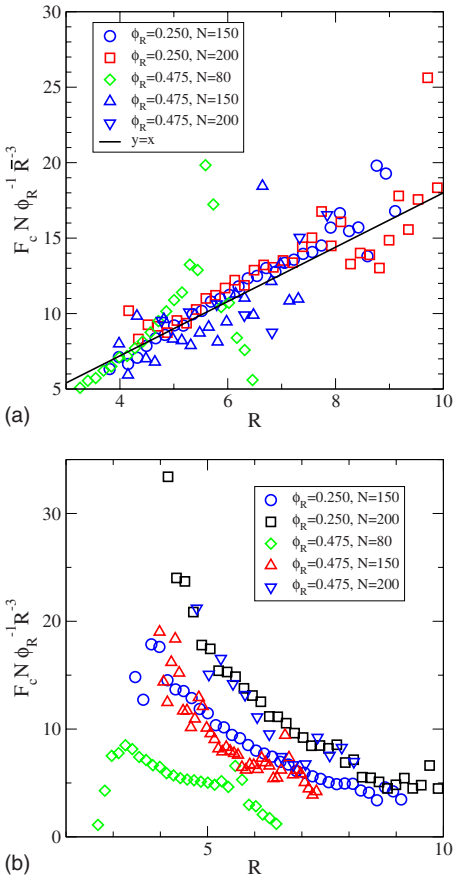

FIG. 10. (Color online) (a) The mean-field scaling proposed earlier [14] that assumes that all RPs are of the same size. (b) The free energy of catenation obtained from this study cast in the form proposed in [7] seems to be correct only in the limit of large R.

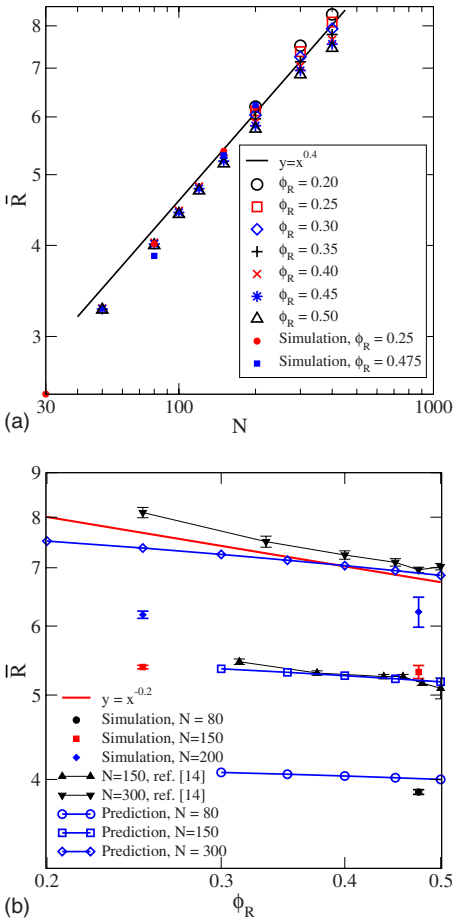

FIG. 11. (Color online) The average radius of gyration $\bar{R}$ obtained using the regressed formula for $F_c(R|N;\phi_R)$. The average radius of gyration $\bar{R}$ obtained from the simulations (valid false rings) and previous work [14] is plotted for comparison. The scaling of $\bar{R}$ as a function of N seems to be captured correctly, but its dependence on ϕ seems more like $\bar{R} \sim \phi^{-0.14}$.

regimes scales as $\phi_R^* \sim N^{-1/2}$. The value of ϕ_R^* was reported as 0.27 and 0.17 for $N=150$ and $N=300$, respectively [14]. Using this information, we obtain $\phi_R^* = 3.13/\sqrt{N}$, and only those systems in the semidilute regime were considered.

To test the effect of catenation on the free energy, Fig. 10(a) shows a plot of the free energy of catenation normalized according to the scaling in Eq. (3), where the mean value of the radius of gyration $\bar{R}$ is used, instead of R. It is observed that the normalized free energy of an RP has a distinct seemingly linear dependence on the polymer size when plotted in this manner. If the Cates-Deustch expression for the free energy due to catenation were valid for the systems studied here, then we would expect $F_c N/\phi_R R^3$ to be approximately constant. However as shown in Fig. 10(b), this holds true only as R becomes large. Performing a multiple linear regression it is found that $F_c = 0.066 \phi_R^{0.91} N^{0.51} R^{1.35}$

It must be noted at this point that the variable R in the regressed expression for F_c does *not* refer to the mean radius of gyration of all RPs in the melt. Instead, it refers to the radius of gyration of a *single* ring polymer, and thus, the expression for F_c is in a sense a measure of the "pressure" that an RP feels as a function of its neighborhood ϕ_R, its molecular weight N, and its size R. Thus, for a single RP, as either of (a) the number RPs in its vicinity, or (b) its molecular weight, or (c) its size, are increased, the RP under consideration feels an increasing "pressure." We expect that this functional form might be different for large N.

$F_g(R|N)$ may be constructed from Eq. (16) to yield the total free energy since the simulation results seem to agree with the analytical results when the catenation constraint is relaxed. From the total free energy, $F(R|N;\phi_R)$, the average radius of gyration is then computed as

$$\bar{R}(N,\phi_R) = \frac{\int_0^\infty R \exp[-F(R|N;\phi_R)]dR}{\int_0^\infty \exp[-F(R|N;\phi_R)]dR}. \quad (17)$$

Figures 11(a) and 11(b) depict the variation in $\bar{R}(N,\phi_R)$ with N and ϕ_R, computed using the PDF of R obtained from all false rings to obtain $F_g(R|N)$, and the regressed expression for $F_c(R|N;\phi_R)$ over different molecular weights and fractions of RPs in the semidilute regime. Overlaid on these plots are the values of $\bar{R}$ obtained from the simulations in this

work, and previously published data [14]. While the agreement between the predicted $\bar{R}$ values and the observed $\bar{R}$ values seems reasonable, there are some ambiguities that should be pointed out.

In this work, the values of $\bar{R}$ predicted using the regressed expression for $F_c(R|N;\phi_R)$ seems to have the correct dependence on N. The observed dependence on ϕ_R, however, seems stronger than the predicted dependence. In addition to this, the prediction overestimates $\bar{R}$ for $N=80$, and underestimates $\bar{R}$ for $N=300$. This result was originally thought to be the result of having insufficient sampling of valid ring conformations. Thus, a different set of traditional S-BFM simulations of ring-linear blends, wherein the rings are not allowed to cross each other, were executed to obtain a more robust estimate of the PDF of valid rings, $P(R|N;\phi_R)$. However, the PDFs obtained in this fashion were found to closely match the PDFs obtained from the entropy simulations, and did not appreciably affect the regressed expression for F_c. Thus, the error might lie in estimating the probability of forming a valid ring, λ^V. We attribute this to having insufficient sampling at large ϕ_R. Indeed, as seen in Fig. 6, most of the data that we have is close to the regime in which the transition from dilute to semidilute takes place.

It is useful at this point to recall that the scaling argument of Iyer *et al.* [14] leads to $\bar{R}(N,\phi_R)\sim N^{\nu}\phi_R^{2\nu-1}$, which is a generalization of the Cates-Deutsch argument for which $\nu=0.4$. It was seen earlier [14] that the S-BFM model yields $\nu=0.43$, which is consistent with a scaling of $\bar{R}\sim\phi^{-0.14}$, and this is the scaling seen in Fig. 11(b). In their simulations, Iyer *et al.*, found $\bar{R}(N,\phi_R)\sim N^{0.43}\phi_R^{-0.2}$, while the expression for the free energy developed in this work yields $\bar{R}(N,\phi_R)\sim N^{0.40}\phi_R^{-0.14}$. Thus, there is a mismatch of exponents from these two studies in relation to the scaling model, and at this point we do not have a clear idea of its origin.

In terms of computational time and effort, it becomes increasingly difficult to probe the semidilute regime with increasing N. This is because the chances of observing a valid false ring diminish rapidly as ϕ_R and N increase. There are three reasons for this: (1) at large ϕ_R, the number of LPs in the simulation box is small, thereby reducing the number of possible false rings, (2) the probability with which an LP forms a false ring decreases rapidly with increasing N. Indeed, as seen in Fig. 4, $\lambda^A\sim N^{-1.56}$, and (3) as ϕ_R increases, the number of true rings that an LP can thread through is far greater than at low ϕ_R. Thus, in terms of obtaining the probability of forming a valid false ring, λ^V, probing the semidilute regime requires simulations at large N and ϕ_R, which become prohibitively expensive. Since λ^V is one of the key pieces of information required to compute the free energy of catenation, we believe that the regressed expression for F_c presented in this work may be weighted less by the actual semidilute regime, and more by the transition regime from dilute to semidilute, and might suffer in part from finite size effects.

It has also been seen that the approach to asymptotic behavior (large values of N) can be quite slow [26], thereby presenting a significant computational hurdle toward obtaining accurate statistics from the true semidilute regime. Obukhov *et al.* [26] reported that the exponent $\nu=2/5$ predicted by the Cates-Deutsch argument [7] might be at best an upper limit for a ring polymer in a melt. Other numerical studies for large molecular weights have obtained results consistent with this argument. One of the studies, by Müller *et al.* [24], who studied using a different bond-fluctuation model, the CK-BFM [29], molecular weights up to $N=1024$ (this corresponds to $N\approx 410$ in the S-BFM [9]), found a value of the exponent ν between 0.33 and 0.4. Another more recent study by Vettorel *et al.* [25] studied molecular weights up to 10082 on a simple cubic lattice (as in this study), and obtained results that indicate that $\nu\approx 0.3$. In view of the slow approach to asymptotic behavior, it is stressed that the exponents in the expressions for free energy presented in this paper might be valid only for the low molecular weight N regime, and might change as N increases.

V. CONCLUSIONS

The S-BFM model was used to execute simulations of ring-linear polymer melts at varying ring fractions. The probability with which LPs adopt configurations that makes them indistinguishable from rings was determined and used to compute the conformational free energy of RPs at various concentrations of rings. Previously proposed scalings ($F_c\sim\phi_R N^{-1}R^3$) were shown to be valid only in a mean-field sense, and alternate forms were investigated. The data in this study was used to propose a new scaling for the free energy of catenation of RPs in a ring-linear blend as $F_c\sim\phi_R^{0.91}N^{0.51}R^{1.35}$. This scaling may require modification, as it does not predict the dependence of $\bar{R}$ as a function of ϕ_R accurately. We attribute this to having insufficient sampling at high ϕ_R and N. It is also possible that the *total* free energy, F_g+F_c cannot be captured accurately by a simple scaling argument as the Gaussian part F_g has a complex dependence on molecular weight.

ACKNOWLEDGMENTS

Partial support for this work was provided by the Petroleum Research Foundation of the American Chemical Society through ACS PRF Grant No. 46770-G7. The authors wish to thank Professor DeWitt Sumners of the Mathematics department at Florida State University for helpful discussions on the linking number.

TABLE I. Table summarizing the test cases to compare results from annealing with those obtained using linking number.

		Catenated Rings			
N	ϕ_R	Total rings formed	Annealing	Linking number	% difference
30	0.250	190766	67949	67945	0.006
30	0.475	10351	5947	5945	0.034

APPENDIX

To determine whether the linking number algorithm used in this study yields results comparable with the annealing algorithm, a test simulation with two different ϕ_R values was executed. Periodically, false rings were examined for catenation with true rings by both the annealing algorithm and linking number algorithm. These test cases are summarized in Table I. It may be seen that for the test cases, differences in the results between annealing and linking number is less than 0.1%. Furthermore, as some of the rings declared as catenated by annealing may be attributed to insufficient annealing time, it may be concluded that the linking number algorithm performs exceedingly well for purposes of this paper.

[1] J. A. Semlyen, *Cyclic Polymers*, 2nd ed. (Springer, Dordrecht, 2000).
[2] H.-X. Zhou, J. Mol. Biol. **332**, 257 (2003).
[3] H.-X. Zhou, J. Am. Chem. Soc. **125**, 9280 (2003).
[4] W. Carl, J. Chem. Soc., Faraday Trans. **91**, 2525 (1995).
[5] A. J. Spakowitz, EPL **73**, 684 (2006).
[6] J. Roovers, Macromolecules **18**, 1359 (1985).
[7] M. E. Cates and J. M. Deutsch, J. Phys. (Paris) **47**, 2121 (1986).
[8] G. B. McKenna, G. Hadziioannou, P. Lutz, G. Hild, C. Strazielle, C. Straupe, P. Rempp, and A. J. Kovacs, Macromolecules **20**, 498 (1987).
[9] G. Subramanian and S. Shanbhag, Phys. Rev. E **77**, 011801 (2008).
[10] S. J. Spengler, A. Stasiak, and N. R. Cozzarelli, Cell **42**, 325 (1985).
[11] D. W. Sumners, Notices of the AMS **42**, 528 (1995).
[12] A. V. Vologodskii, N. J. Crisona, B. Laurie, P. Pieranski, V. Katritch, J. Dubochet, and A. Stasiak, J. Mol. Biol. **278**, 1 (1998).
[13] G. B. McKenna and D. J. Plazek, Polym. Commun. **27**, 304 (1986).
[14] B. V. S. Iyer, A. K. Lele, and S. Shanbhag, Macromolecules **40**, 5995 (2007).
[15] D. Kawaguchi, K. Masuoka, A. Takano, K. Tanaka, T. Nagamura, N. Torikai, R. M. Dalgliesh, S. Langridge, and Y. Matsushita, Macromolecules **39**, 5180 (2006).
[16] G. Subramanian and S. Shanbhag, Macromolecules **41**, 7239 (2008).
[17] R. M. Robertson and D. E. Smith, Macromolecules **40**, 3373 (2007).
[18] M. Kapnistos, M. Lang, D. Vlassopoulos, W. Pyckhout-Hintzen, D. Richter, D. Cho, T. Chang, and M. Rubinstein, Nature Mater. **7**, 997 (2008).
[19] S. Geyler and T. Pakula, Makromol. Chem., Rapid Commun. **9**, 617 (1988).
[20] M. Müller, J. P. Wittmer, and M. E. Cates, Phys. Rev. E **53**, 5063 (1996).
[21] S. Brown and G. Szamel, J. Chem. Phys. **108**, 4705 (1998).
[22] V. Arrighi, S. Gagliardi, A. C. Dagger, J. A. Semlyen, J. S. Higgins, and M. J. Shenton, Macromolecules **37**, 8057 (2004).
[23] J. Suzuki, A. Takano, and Y. Matsushita, J. Chem. Phys. **129**, 034903 (2008).
[24] M. Müller, J. P. Wittmer, and M. E. Cates, Phys. Rev. E **61**, 4078 (2000).
[25] T. Vettorel, A. Y. Grosberg, and K. Kremer, Phys. Biol. **6**, 025013 (2009).
[26] S. P. Obukhov, M. Rubinstein, and T. Duke, Phys. Rev. Lett. **73**, 1263 (1994).
[27] A. Takano, Polym. Prepr. Jpn **56**, 2424 (2007).
[28] J. S. Shaffer, J. Chem. Phys. **101**, 4205 (1994).
[29] I. Carmesin and K. Kremer, Macromolecules **21**, 2819 (1988).
[30] G. Subramanian and S. Shanbhag, J. Chem. Phys. **129**, 144904 (2008).
[31] R. Everaers, S. K. Sukumaran, G. S. Grest, C. Svaneborg, A. Sivasubramanian, and K. Kremer, Science **303**, 823 (2004).
[32] S. Shanbhag and R. G. Larson, Phys. Rev. Lett. **94**, 076001 (2005).
[33] V. F. R. Jones, *A Polynomial Invariant for Knots via von Neumann Algebras*, Fields Medallists' Lectures (World Scientific, Singapore, 1997).
[34] C. C. Adams, *The Knot Book* (American Mathematical Society, Providence, 2004).
[35] S. Shanbhag and M. Kroger, Macromolecules **40**, 2897 (2007).
[36] J. S. Shaffer, J. Chem. Phys. **103**, 761 (1995).
[37] C. F. Gauss, *Werke: Königliche Gesellschaft der Wissenschaften* (Teubner, Göttingen, 1833).
[38] D. Frenkel and B. Smit, *Understanding Molecular Simulation: From Algorithms to Applications*, 2nd ed. (Academic Press, Orlando, FL, 2002).
[39] R. C. Lua, A. L. Borovinskiy, and A. Y. Grosberg, Polymer **45**, 717 (2004).
[40] R. C. Lua (private communication).
[41] J. H. C. Whitehead, *The Mathematical Works of J. H. C. Whitehead* (Pergamon Press, New York, 1963).
[42] T. Minato and A. Hatano, J. Phys. Soc. Jpn. **42**, 1992 (1977).
[43] S. Brown, T. Lenczycki, and G. Szamel, Phys. Rev. E **63**, 052801 (2001).